

Manuscript

*Local density approximation in site-occupation embedding theory*Bruno Senjean¹, Masahisa Tsuchiizu², Vincent Robert¹, and Emmanuel Fromager^{1*}¹*Laboratoire de Chimie Quantique, Institut de Chimie, CNRS / Université de Strasbourg,
4 rue Blaise Pascal, 67000 Strasbourg, France*²*Department of Physics, Nagoya University, Nagoya 464-8602, Japan**(Received 00 Month 200x; final version received 00 Month 200x)*

Site-occupation embedding theory (SOET) is a density-functional theory (DFT)-based method which aims at modelling strongly correlated electrons. It is in principle exact and applicable to model and quantum chemical Hamiltonians. The theory is presented here for the Hubbard Hamiltonian. In contrast to conventional DFT approaches, the site (or orbital) occupations are deduced in SOET from a partially-interacting system consisting of one (or more) impurity site(s) and non-interacting bath sites. The correlation energy of the bath is then treated implicitly by means of a site-occupation functional. In this work, we propose a simple impurity-occupation functional approximation based on the two-level (2L) Hubbard model which is referred to as two-level impurity local density approximation (2L-ILDA). Results obtained on a prototypical uniform 8-site Hubbard ring are promising. The extension of the method to larger systems and more sophisticated model Hamiltonians is currently in progress.

Keywords: Density functional theory, Site-occupation embedding theory, Strongly correlated electrons, Hubbard Hamiltonian.

1. Introduction

Modelling strongly correlated electronic systems, such as materials and molecules containing transition metals, remains a challenge for quantum chemists and condensed matter physicists. The difficulty lies in the proper description of both strong (static) and weak (dynamical) correlation effects. Strong correlation prevents from using a mean-field approximation as starting point for the description of the dynamical correlation. While, in computational chemistry, multi-reference perturbation and coupled-cluster theories (see, for example, Refs. [1–5]) became the state of the art, various methods have also been developed in condensed matter physics. Let us mention, among others, quantum and variational Monte Carlo [6–11], the density-matrix renormalization group (DMRG) method [12, 13], the symmetry breaking and restoration methods [14–19] and methods based on the Gutwiller variational approach [20, 21]. Considering that electron correlation is local [22–25], alternative approaches such as the dynamical mean-field theory (DMFT) [26–30] decompose the whole system into a small subsystem called impurity, which is embedded in the rest of the system referred to as the bath. The impurity and the bath interact with each other in some approximate but

*Corresponding author. Email: fromagere@unistra.fr

self-consistent way. DMFT as well as the recently proposed self-energy embedding theory (SEET) [31, 32] are formulated in terms of the (frequency-dependent) one-particle Green's function. In the latter case, the self-energy for the strongly correlated orbitals (corresponding to the local correlation effects) is obtained from an exact diagonalisation, which is equivalent to full configuration interaction (FCI), and the remaining part of the correlation (called non-local correlation) is modelled with a self-consistent second-order Green's function method (GF2) [33, 34].

Chan and coworkers [35, 36] recently introduced a density-matrix embedding theory (DMET) which builds an embedded impurity model from the (frequency-independent) one-particle density matrix. Such an approach enables the computation of ground-state properties at a much lower computational cost. Bulik *et al.* [37] proposed a simplified version of DMET, referred to as density embedding theory (DET), which uses the diagonal elements of the density matrix only. In DMET, the quantum impurity solver can be the FCI method, and the bath is treated in a mean-field approximation such as Hartree–Fock (this is called FCI-in-HF embedding in Ref. [25]). In order to overcome such limitations, Tsuchimochi *et al.* [25] proposed to use an antisymmetrized geminal power (AGP) [38–40] wave function for the bath.

In this paper, we explore an alternative frequency-independent embedding scheme, called site-occupation embedding theory (SOET), which has been introduced recently by one of the authors [41]. SOET is a density-functional theory (DFT)-based method. More precisely, it relies on the extension of DFT to model Hamiltonians [42–46], which is often referred to as site-occupation functional theory (SOFT). Note that SOET can in principle be adapted to quantum chemical Hamiltonians [41]. The difference between conventional SOFT and SOET lies in the choice of the fictitious system from which the site occupations are obtained. In SOET, a partially-interacting system consisting of an interacting impurity site and non-interacting bath sites is considered, rather than a completely non-interacting system. The embedding of the impurity system is in principle exact and obtained from a site-occupation correlation functional for the bath. So far, SOET has been explored at the formal level only [41]. In particular, no explicit site-occupation approximate functional was derived. In this work, we propose a simple local density approximation (LDA) based on the Hubbard dimer.

The paper is organized as follows: After a brief introduction to SOFT (Section 2.1) and SOET (Section 2.2), the application of SOET to the two-electron Hubbard dimer is discussed in details in Section 2.3. An impurity-occupation functional approximation based on the Hubbard dimer is then introduced in Section 2.4. After the computational details (Section 3), exact and approximate results obtained for uniform 8-site Hubbard rings are presented in Section 4. Conclusions are given in Section 5.

2. Theory

2.1. Site-occupation functional theory

Let us consider the second-quantized expression for the Hubbard model Hamiltonian with an external potential $\mathbf{v} \equiv \{v_i\}_i$,

$$\begin{aligned}\hat{H} &= \hat{\mathcal{T}} + \hat{U} + \sum_i v_i \hat{n}_i, \\ \hat{\mathcal{T}} &= -t \sum_{\langle i,j \rangle, \sigma} \hat{a}_{i\sigma}^\dagger \hat{a}_{j\sigma}, \\ \hat{U} &= U \sum_i \hat{n}_{i\uparrow} \hat{n}_{i\downarrow},\end{aligned}\tag{1}$$

where $t > 0$ is the hopping integral, $U > 0$ is the on-site two-electron repulsion parameter, $\hat{n}_{i\sigma} = \hat{a}_{i\sigma}^\dagger \hat{a}_{i\sigma}$, and $\sigma = \uparrow, \downarrow$. The site-occupation operator equals $\hat{n}_i = \hat{n}_{i\uparrow} + \hat{n}_{i\downarrow}$ and, for a given wave function Ψ , the occupation of site i is defined as $n_i = \langle \Psi | \hat{n}_i | \Psi \rangle$. As shown by Gunnarsson and Schönhammer [44], the Hohenberg–Kohn (HK) theorem can be adapted to the Hamiltonian in Equation (1), i.e. there is a one-to-one correspondence between the external potential \mathbf{v} , up to a constant, and the ground-state site occupations $\mathbf{n} \equiv \{n_i\}_i$. Consequently, for a given potential \mathbf{v} , the exact ground-state energy $E(\mathbf{v})$ can be obtained from the following variational principle,

$$E(\mathbf{v}) = \min_{\mathbf{n}} \left\{ F(\mathbf{n}) + (\mathbf{v}|\mathbf{n}) \right\},\tag{2}$$

where $(\mathbf{v}|\mathbf{n}) = \sum_i v_i n_i$. In this approach, which is referred to as the site-occupation functional theory (SOFT) in the following, the analog of the universal HK functional is a t - and U -dependent functional of the site occupations that can be written within the Levy–Lieb (LL) constrained-search formalism as

$$F(\mathbf{n}) = \min_{\Psi \rightarrow \mathbf{n}} \left\{ \langle \Psi | \hat{\mathcal{T}} + \hat{U} | \Psi \rangle \right\}.\tag{3}$$

Note that the site occupations are a collection of occupation numbers whereas the electron density, which is the basic variable in conventional DFT, is a continuous function of space coordinates. Strictly speaking, one should refer to $F(\mathbf{n})$ as a LL function rather than functional. Nevertheless, "functional" is often used in the literature [43], thus emphasizing on the formal analogies between SOFT and DFT. We will do the same in the rest of this paper. Note that the LL functional can be rewritten as a Legendre–Fenchel transform [41, 47]:

$$F(\mathbf{n}) = \sup_{\mathbf{v}} \left\{ E(\mathbf{v}) - (\mathbf{v}|\mathbf{n}) \right\}.\tag{4}$$

The maximising potential provides the ground-state wave function with site occupations \mathbf{n} . As shown in Sec. 2.3, this expression is very convenient for computing exact correlation energies in simple systems like the Hubbard dimer.

The Kohn–Sham (KS) formulation of SOFT (KS–SOFT) is obtained from

the following partitioning,

$$F(\mathbf{n}) = \mathcal{T}_s(\mathbf{n}) + E_{\text{Hxc}}(\mathbf{n}), \quad (5)$$

where the non-interacting kinetic energy functional is defined in analogy with KS-DFT as

$$\mathcal{T}_s(\mathbf{n}) = \min_{\Psi \rightarrow \mathbf{n}} \left\{ \langle \Psi | \hat{T} | \Psi \rangle \right\}, \quad (6)$$

and $E_{\text{Hxc}}(\mathbf{n})$ is the Hartree-exchange-correlation (Hxc) site-occupation functional, which can be decomposed into a Hartree-exchange and a correlation part as follows [43],

$$E_{\text{Hxc}}(\mathbf{n}) = E_{\text{Hx}}(\mathbf{n}) + E_c(\mathbf{n}), \quad (7)$$

where

$$E_{\text{Hx}}(\mathbf{n}) = \frac{U}{4} \sum_i n_i^2. \quad (8)$$

The exact expression for the correlation functional is unknown. At the LDA level, which is exact for the uniform Hubbard model, the site-occupation correlation functional is written as

$$E_c^{\text{LDA}}(\mathbf{n}) = \sum_i e_c(n_i), \quad (9)$$

where an approximate expression for the per-site correlation energy $e_c(n)$ can be obtained, for example, from the Bethe-ansatz (BA) solution, thus leading to the BALDA functional of Capelle and coworkers [45]. More on practical KS-SOFT calculations can be found in Refs. [43, 46] and the references therein.

2.2. Site-occupation embedding theory

In the spirit of DMET [35, 37], Fromager [41] proposed recently to treat the two-electron repulsion U explicitly on a limited number of sites called *impurities* while the remaining sites, which play the role of a *bath*, are treated within SOFT, hence this theory is named site-occupation embedding theory (SOET). In the following, we will consider only one impurity site labelled as j_0 . Let us stress that SOET is in principle exact and that the ground-state energy should not depend on the number of impurity sites if exact complementary functionals are used [41]. The exact embedding relies on the following partitioning of the LL functional,

$$F(\mathbf{n}) = F^{\text{imp}}(\mathbf{n}) + \overline{E}_{\text{Hxc}}^{\text{bath}}(\mathbf{n}), \quad (10)$$

where

$$F^{\text{imp}}(\mathbf{n}) = \min_{\Psi \rightarrow \mathbf{n}} \left\{ \langle \Psi | \hat{T} + U \hat{n}_{j_0 \uparrow} \hat{n}_{j_0 \downarrow} | \Psi \rangle \right\}. \quad (11)$$

Note that the latter functional can be rewritten as a Legendre–Fenchel transform [41],

$$F^{\text{imp}}(\mathbf{n}) = \sup_{\mathbf{v}} \left\{ \mathcal{E}^{\text{imp}}(\mathbf{v}) - (\mathbf{v}|\mathbf{n}) \right\}, \quad (12)$$

where

$$\mathcal{E}^{\text{imp}}(\mathbf{v}) = \min_{\Psi} \left\{ \langle \Psi | \hat{\mathcal{T}} + U \hat{n}_{j_0 \uparrow} \hat{n}_{j_0 \downarrow} | \Psi \rangle + (\mathbf{v}|\mathbf{n}^{\Psi}) \right\}, \quad (13)$$

$(\mathbf{v}|\mathbf{n}^{\Psi}) = \langle \Psi | \sum_i v_i \hat{n}_i | \Psi \rangle = \sum_i v_i n_i^{\Psi}$, and \mathbf{n}^{Ψ} denotes the on-site occupations for the trial wave function Ψ . Let us stress that $\mathcal{E}^{\text{imp}}(\mathbf{v})$ is a (non-physical) auxiliary N -electron energy. The maximising potential in Equation (12), which we will refer to as embedding potential in the following, ensures that the fictitious embedded impurity system has the site occupations \mathbf{n} .

Returning to the decomposition in Equation (10), the complementary site-occupation functional for the bath $\bar{E}_{\text{Hxc}}^{\text{bath}}(\mathbf{n})$ depends on t and U only. It is, in a sense, universal as it does not depend on the external potential. In analogy with Equations (7) and (8), we decompose the bath functional as follows,

$$\bar{E}_{\text{Hxc}}^{\text{bath}}(\mathbf{n}) = \bar{E}_{\text{Hx}}^{\text{bath}}(\mathbf{n}) + \bar{E}_{\text{c}}^{\text{bath}}(\mathbf{n}), \quad (14)$$

where

$$\bar{E}_{\text{Hx}}^{\text{bath}}(\mathbf{n}) = \frac{U}{4} \sum_{i \neq j_0} n_i^2. \quad (15)$$

The correlation functional for the bath $\bar{E}_{\text{c}}^{\text{bath}}(\mathbf{n})$ can be connected with the standard correlation functional in Equation (7) by considering the KS partitioning of the embedded impurity LL functional (see Equation (11)),

$$F^{\text{imp}}(\mathbf{n}) = \mathcal{T}_s(\mathbf{n}) + E_{\text{Hxc}}^{\text{imp}}(\mathbf{n}), \quad (16)$$

where the Hxc energy of the embedded impurity equals

$$E_{\text{Hxc}}^{\text{imp}}(\mathbf{n}) = E_{\text{Hx}}^{\text{imp}}(\mathbf{n}) + E_{\text{c}}^{\text{imp}}(\mathbf{n}), \quad (17)$$

with

$$E_{\text{Hx}}^{\text{imp}}(\mathbf{n}) = \frac{U}{4} n_{j_0}^2. \quad (18)$$

Combining Equations (5), (10) and (16) leads to the final expression:

$$\bar{E}_{\text{c}}^{\text{bath}}(\mathbf{n}) = E_{\text{c}}(\mathbf{n}) - E_{\text{c}}^{\text{imp}}(\mathbf{n}). \quad (19)$$

Therefore, in order to perform practical SOET calculations, it is necessary to develop approximations to the impurity correlation functional $E_{\text{c}}^{\text{imp}}(\mathbf{n})$, in addition to the conventional (fully-interacting) correlation functional. For the latter, the BALDA functional [45] could be used. This choice will be discussed in a separate work. In this paper, we focus on approximate impurity correlation functionals

that depend only on the impurity occupation.

Returning to the exact theory, it comes from Equations (2), (10) and (11) that, for any normalised trial wave function Ψ ,

$$\begin{aligned} \langle \Psi | \hat{\mathcal{T}} + U \hat{n}_{j_0\uparrow} \hat{n}_{j_0\downarrow} | \Psi \rangle + \bar{E}_{\text{Hxc}}^{\text{bath}}(\mathbf{n}^\Psi) + (\mathbf{v} | \mathbf{n}^\Psi) &\geq F^{\text{imp}}(\mathbf{n}^\Psi) + \bar{E}_{\text{Hxc}}^{\text{bath}}(\mathbf{n}^\Psi) + (\mathbf{v} | \mathbf{n}^\Psi) \\ &\geq E(\mathbf{v}), \end{aligned} \quad (20)$$

thus leading to the exact variational expression for the ground-state energy:

$$\begin{aligned} E(\mathbf{v}) &= \min_{\Psi} \left\{ \langle \Psi | \hat{\mathcal{T}} + U \hat{n}_{j_0\uparrow} \hat{n}_{j_0\downarrow} | \Psi \rangle + \bar{E}_{\text{Hxc}}^{\text{bath}}(\mathbf{n}^\Psi) + (\mathbf{v} | \mathbf{n}^\Psi) \right\} \\ &= \langle \Psi^{\text{imp}} | \hat{\mathcal{T}} + U \hat{n}_{j_0\uparrow} \hat{n}_{j_0\downarrow} | \Psi^{\text{imp}} \rangle + \bar{E}_{\text{Hxc}}^{\text{bath}}(\mathbf{n}^{\Psi^{\text{imp}}}) + (\mathbf{v} | \mathbf{n}^{\Psi^{\text{imp}}}). \end{aligned} \quad (21)$$

The minimising wave function Ψ^{imp} fulfills the following self-consistent Equation [41]:

$$\left(\hat{\mathcal{T}} + U \hat{n}_{j_0\uparrow} \hat{n}_{j_0\downarrow} + \sum_i \left[v_i + \frac{\partial \bar{E}_{\text{Hxc}}^{\text{bath}}(\mathbf{n}^{\Psi^{\text{imp}}})}{\partial n_i} \right] \hat{n}_i \right) | \Psi^{\text{imp}} \rangle = \mathcal{E}^{\text{imp}} | \Psi^{\text{imp}} \rangle, \quad (22)$$

where \mathcal{E}^{imp} is the energy of the embedded impurity system. Consequently, the exact embedding potential can be expressed as follows,

$$v_i^{\text{emb}} = v_i + \frac{\partial \bar{E}_{\text{Hxc}}^{\text{bath}}(\mathbf{n}^{\Psi^{\text{imp}}})}{\partial n_i}. \quad (23)$$

The latter ensures that the physical (fully-interacting) and fictitious embedded impurity systems have exactly the same site occupations.

2.3. Application to the Hubbard dimer

2.3.1. Notations and energy expressions

In the spirit of a recent work by Carrascal *et al.* [46], we propose in this section to apply SOET to the two-electron Hubbard dimer. For that purpose, we consider the general Hamiltonian expression:

$$\begin{aligned} \hat{\mathcal{H}} &= -t \sum_{\sigma} \left(\hat{a}_{0\sigma}^{\dagger} \hat{a}_{1\sigma} + \hat{a}_{1\sigma}^{\dagger} \hat{a}_{0\sigma} \right) + U_0 \hat{n}_{0\uparrow} \hat{n}_{0\downarrow} \\ &\quad + U_1 \hat{n}_{1\uparrow} \hat{n}_{1\downarrow} + v_0 \hat{n}_0 + v_1 \hat{n}_1. \end{aligned} \quad (24)$$

Let us mention that the uniform case ($n_0 = n_1 = 1$) has already been solved in Ref. [41]. For simplicity, we will assume that

$$v_0 + v_1 = 0. \quad (25)$$

Note that the latter condition is fulfilled by any potential once it has been shifted by $-(v_0 + v_1)/2$. The physical and non-interacting KS systems are obtained when $U_0 = U_1 = U$ and $U_0 = U_1 = 0$, respectively. The embedded impurity system, where the impurity site is labelled as 0, corresponds to $U_0 = U$ and $U_1 = 0$.

Since we are interested in the singlet ground state only, the matrix representation of the Hamiltonian can be reduced to the basis of the "doubly-occupied site" states $|D_i\rangle = \hat{a}_{i\uparrow}^\dagger \hat{a}_{i\downarrow}^\dagger |\text{vac}\rangle$ with $i = 0$ or 1 , and $|S\rangle = 1/\sqrt{2}(\hat{a}_{0\uparrow}^\dagger \hat{a}_{1\downarrow}^\dagger - \hat{a}_{0\downarrow}^\dagger \hat{a}_{1\uparrow}^\dagger) |\text{vac}\rangle$ that corresponds to singly-occupied sites, thus leading to [41]:

$$[\hat{\mathcal{H}}] = \begin{bmatrix} U_0 - \delta v & 0 & -\sqrt{2}t \\ 0 & U_1 + \delta v & -\sqrt{2}t \\ -\sqrt{2}t & -\sqrt{2}t & 0 \end{bmatrix}, \quad (26)$$

where $\delta v = v_1 - v_0$. For a physical system ($U_0 = U_1 = U$), the exact ground-state energy can be expressed analytically as follows [46],

$$E(U, \delta v) = \frac{4t}{3} \left(u - w \sin \left(\theta + \frac{\pi}{6} \right) \right), \quad (27)$$

where

$$u = U/2t, \quad (28)$$

$$w = \sqrt{3(1 + \nu^2) + u^2}, \quad (29)$$

$$\nu = \delta v/2t, \quad (30)$$

and

$$\cos(3\theta) = (9(\nu^2 - 1/2) - u^2) u/w^3. \quad (31)$$

The expression for the exact ground-state energy $\mathcal{E}(U_0, U_1, \delta v)$ of the general Hamiltonian matrix in Equation (26) is then obtained straightforwardly by considering an effective physical system such that

$$\begin{aligned} U_{\text{eff}} - \delta v_{\text{eff}} &= U_0 - \delta v, \\ U_{\text{eff}} + \delta v_{\text{eff}} &= U_1 + \delta v, \end{aligned} \quad (32)$$

or, equivalently,

$$U_{\text{eff}} = \frac{U_0 + U_1}{2}, \quad (33)$$

$$\delta v_{\text{eff}} = \delta v + \frac{U_1 - U_0}{2}. \quad (34)$$

As a result, we obtain the final expression:

$$\mathcal{E}(U_0, U_1, \delta v) = E\left((U_0 + U_1)/2, \delta v + (U_1 - U_0)/2\right). \quad (35)$$

In the particular case of the embedded impurity system, the energy becomes

$$\mathcal{E}^{\text{imp}}(U, \delta v) = \mathcal{E}(U, 0, \delta v) = E(U/2, \delta v - U/2). \quad (36)$$

For conveniency, the occupation of site 0 will be denoted as $n_0 = n$. Consequently, $n_1 = 2 - n$ since the number of electrons is held constant and equal to 2. Therefore, in this simple system, the site occupations reduce to a single number n which can vary from 0 to 2.

2.3.2. Non-interacting and physical systems

As shown in Ref. [46], the non-interacting kinetic energy and the KS potential can be expressed analytically as follows,

$$\mathcal{T}_s(n) = -2t\sqrt{n(2-n)}, \quad (37)$$

and

$$\delta v^{\text{KS}}(n) = \frac{\partial \mathcal{T}_s(n)}{\partial n} = \frac{2t(n-1)}{\sqrt{n(2-n)}}. \quad (38)$$

On the other hand, there is no simple analytical expression for the fully-interacting LL functional. Nevertheless, the latter can be computed "exactly" by means of the Legendre–Fenchel transform in Equation (4). Using Equation (25) leads to the final expression:

$$\begin{aligned} F(U, n) &= \sup_{\delta v} \left\{ E(U, \delta v) + \delta v \times (n-1) \right\} \\ &= E(U, \delta v(U, n)) + \delta v(U, n) \times (n-1). \end{aligned} \quad (39)$$

Note that the maximising potential $\delta v(U, n)$ ensures that the physical ground-state occupation of site 0 equals n . It then becomes possible to compute the exact correlation energy as follows,

$$E_c(U, n) = F(U, n) - \mathcal{T}_s(n) - E_{\text{Hx}}(U, n), \quad (40)$$

where

$$\begin{aligned} E_{\text{Hx}}(U, n) &= \frac{U}{4} (n_0^2 + n_1^2) \\ &= U \left(1 - n(2-n)/2 \right). \end{aligned} \quad (41)$$

Interestingly, as readily seen in Equations (27)–(31), the physical energy is an even function of the potential,

$$E(U, \delta v) = E(U, -\delta v). \quad (42)$$

As a result, the substitution $n \rightarrow 2-n$ in Equation (39) leads to

$$\begin{aligned} F(U, 2-n) &= \sup_{\delta v} \left\{ E(U, -\delta v) - \delta v \times (n-1) \right\} \\ &= E(U, -\delta v(U, 2-n)) - \delta v(U, 2-n) \times (n-1), \end{aligned} \quad (43)$$

which gives, by comparison with Equation (39), the hole/particle symmetry relation for the functional,

$$F(U, 2-n) = F(U, n), \quad (44)$$

and the corresponding antisymmetry relation for the physical potential:

$$\delta v(U, 2 - n) = -\delta v(U, n). \quad (45)$$

Since both the non-interacting kinetic energy and the Hx energy (see Equations (37) and (41)) exhibit the same symmetry,

$$\mathcal{T}_s(2 - n) = \mathcal{T}_s(n), \quad (46)$$

$$E_{\text{Hx}}(U, 2 - n) = E_{\text{Hx}}(U, n), \quad (47)$$

we conclude that

$$E_c(U, 2 - n) = E_c(U, n). \quad (48)$$

In addition, we see from Equation (38) that, for the KS system, the following hole/particle antisymmetry relation is fulfilled:

$$\delta v^{\text{KS}}(2 - n) = -\delta v^{\text{KS}}(n). \quad (49)$$

As a result, the Hxc potential $\delta v_{\text{Hxc}}(U, n) = \delta v^{\text{KS}}(n) - \delta v(U, n)$ fulfills the same antisymmetry relation:

$$\delta v_{\text{Hxc}}(U, 2 - n) = -\delta v_{\text{Hxc}}(U, n). \quad (50)$$

Note that this antisymmetric behavior of the Hxc potential is directly connected to the hole/particle symmetry of the Hxc energy. This appears clearly from the following alternative derivation: according to Equation (39), we have for any trial site occupation ρ ,

$$F(U, \rho) \geq E(U, \delta v(U, n)) + \delta v(U, n) \times (\rho - 1), \quad (51)$$

thus leading to

$$E(U, \delta v(U, n)) = \min_{\rho} \left\{ F(U, \rho) - \delta v(U, n) \times (\rho - 1) \right\}, \quad (52)$$

and, consequently, to

$$\delta v(U, n) = \frac{\partial F(U, n)}{\partial n}. \quad (53)$$

We obtain from Equation (38) the expected expression for the Hxc potential:

$$\begin{aligned} \delta v_{\text{Hxc}}(U, n) &= -\frac{\partial E_{\text{Hxc}}(U, n)}{\partial n} \\ &= \delta v_{\text{Hx}}(U, n) - \frac{\partial E_c(U, n)}{\partial n}, \end{aligned} \quad (54)$$

where $\delta v_{\text{Hx}}(U, n) = U(1 - n)$. Thus, we recover Equation (50) from Equations (47) and (48). Note finally the minus sign on the right-hand side of Equation (54) which is simply related to the fact that $\delta v_{\text{Hxc}}(U, n)$ is the difference between the

Hxc potential values on sites 1 and 0:

$$\left(\frac{\partial E_{\text{Hxc}}(\mathbf{n})}{\partial n_1} - \frac{\partial E_{\text{Hxc}}(\mathbf{n})}{\partial n_0} \right) \bigg|_{n_0=n, n_1=2-n} = -\frac{\partial}{\partial n} [E_{\text{Hxc}}(n, 2-n)] = \delta v_{\text{Hxc}}(U, n), \quad (55)$$

since, by construction, $E_{\text{Hxc}}(n, 2-n) = E_{\text{Hxc}}(U, n)$.

2.3.3. Embedded impurity system

In analogy with Equation (39), the Legendre–Fenchel transform for the embedded impurity system (see Equation (12)) can be rewritten as

$$F^{\text{imp}}(U, n) = \sup_{\delta v} \left\{ \mathcal{E}^{\text{imp}}(U, \delta v) + \delta v \times (n-1) \right\}, \quad (56)$$

where the maximising potential $\delta v^{\text{emb}}(U, n)$ ensures that the ground-state impurity occupation in the embedded impurity system equals n . Using Equations (36) and (39) leads to the following scaling/shifting relations for the functional,

$$F^{\text{imp}}(U, n) = F(U/2, n) + \frac{U}{2}(n-1), \quad (57)$$

and for the maximising potential,

$$\delta v^{\text{emb}}(U, n) = \delta v(U/2, n) + U/2. \quad (58)$$

Consequently, the embedded impurity Hxc potential $\delta v_{\text{Hxc}}^{\text{imp}}(U, n) = \delta v^{\text{KS}}(n) - \delta v^{\text{emb}}(U, n)$ can be expressed as

$$\delta v_{\text{Hxc}}^{\text{imp}}(U, n) = \delta v_{\text{Hxc}}(U/2, n) - U/2. \quad (59)$$

Note that, according to Equation (50), the following hole/particle antisymmetry relation is fulfilled:

$$\delta v_{\text{Hxc}}^{\text{imp}}(U, 2-n) = -\delta v_{\text{Hxc}}^{\text{imp}}(U, n) - U. \quad (60)$$

The correlation energy of the embedded impurity is defined as

$$E_c^{\text{imp}}(U, n) = F^{\text{imp}}(U, n) - \mathcal{T}_s(n) - E_{\text{Hx}}^{\text{imp}}(U, n), \quad (61)$$

where

$$E_{\text{Hx}}^{\text{imp}}(U, n) = \frac{U}{4}n^2. \quad (62)$$

According to Equations (40), (41) and (57), we conclude that the latter correlation energy is simply obtained from the conventional fully-interacting correlation energy by scaling (by 1/2) the U parameter:

$$E_c^{\text{imp}}(U, n) = E_c(U/2, n). \quad (63)$$

This scaling relation provides a remarkably simple connection between SOET and KS-SOFT. Moreover it gives, when combined with Equations (54) and (59), the expected expression

$$\delta v_{\text{Hxc}}^{\text{imp}}(U, n) = -\frac{\partial E_{\text{Hxc}}^{\text{imp}}(U, n)}{\partial n} \quad (64)$$

$$= \delta v_{\text{Hx}}^{\text{imp}}(U, n) - \frac{\partial E_{\text{c}}^{\text{imp}}(U, n)}{\partial n}, \quad (65)$$

where $\delta v_{\text{Hx}}^{\text{imp}}(U, n) = -Un/2$. Note finally that, according to Equation (48), the correlation energy of the embedded impurity fulfills the hole/particle symmetry relation:

$$E_{\text{c}}^{\text{imp}}(U, 2 - n) = E_{\text{c}}^{\text{imp}}(U, n). \quad (66)$$

The "exact" conventional and impurity correlation site-occupation functionals obtained by computing Legendre–Fenchel transforms are shown in Figure 1. The corresponding Hxc potentials are plotted in Figure 2. Scaling as well as hole/particle symmetry and antisymmetry relations are clearly illustrated. Note that the parametrisation of Carrascal *et al.* [46], which is also given in the Figures, provides accurate correlation energies and potentials for all U and n values, as expected. In the following, we will show how it can actually be used in practical SOET calculations. Returning to Figure 2, the deviation from the mean-field approximation (no correlation) becomes significant when U/t increases. Interestingly, correlation effects are slightly attenuated in the embedded impurity system because of the scaling by $1/2$ of the U parameter. This is directly connected to the fact that the bath site is non-interacting.

As already shown by Carrascal *et al.* [46], the potentials exhibit a discontinuity at $n = 1$ (i.e. when both sites are half-filled) in the strongly correlated limit ($U/t \rightarrow +\infty$). A similar discontinuity can be observed in the Anderson junction model [48–50]. It can be interpreted as follows: the impurity site with occupation n is an open system and, in order to let n vary continuously from 0 to 1, we need a grand canonical ensemble consisting of degenerate zero- and one-electron states. The latter states are indeed degenerate (and therefore mixable) if the potential v_0 on the impurity site equals zero. On the other hand, when n varies continuously from 1 to 2, the ensemble should consist of one- and two-electron states. The latter become degenerate if $v_0 = 2v_1 + U$ or, equivalently, if $v_0 = -U$. Since the bath is non-interacting, the potential v_1 can be set to zero for any n values, thus leading to $\delta v^{\text{emb}} = 0$ when $0 < n < 1$ and $\delta v^{\text{emb}} = U$ when $1 < n < 2$. For a non-interacting system, the potential δv^{KS} should be zero for any n so that zero-, one- and two-electron states can be mixed, as illustrated in Figure 9 (right panel) of Ref. [46]. As a result, we conclude that $\delta v_{\text{Hxc}}^{\text{imp}} = \delta v^{\text{KS}} - \delta v^{\text{emb}} = 0$ for $0 < n < 1$ and $\delta v_{\text{Hxc}}^{\text{imp}} = -U$ for $1 < n < 2$, which is in perfect agreement with the bottom panel of Figure 2. For the fully-interacting Hxc potential, we can do a similar analysis: if $0 < n < 1$, then $v_0 = 0$ (so that zero- and one-electron states can be mixed on site 0) and $v_1 = -U$ (so that one- and two-electron states can be mixed on site 1), thus leading to $\delta v = -U$ and $\delta v_{\text{Hxc}} = \delta v^{\text{KS}} - \delta v = U$. When $1 < n < 2$, zero- and one-electron states should mix on site 1 while one- and two-electron states will mix on site 0, thus leading to $v_0 = -U$, $v_1 = 0$, $\delta v = U$ and, consequently, $\delta v_{\text{Hxc}} = -U$, which is again in agreement with the bottom

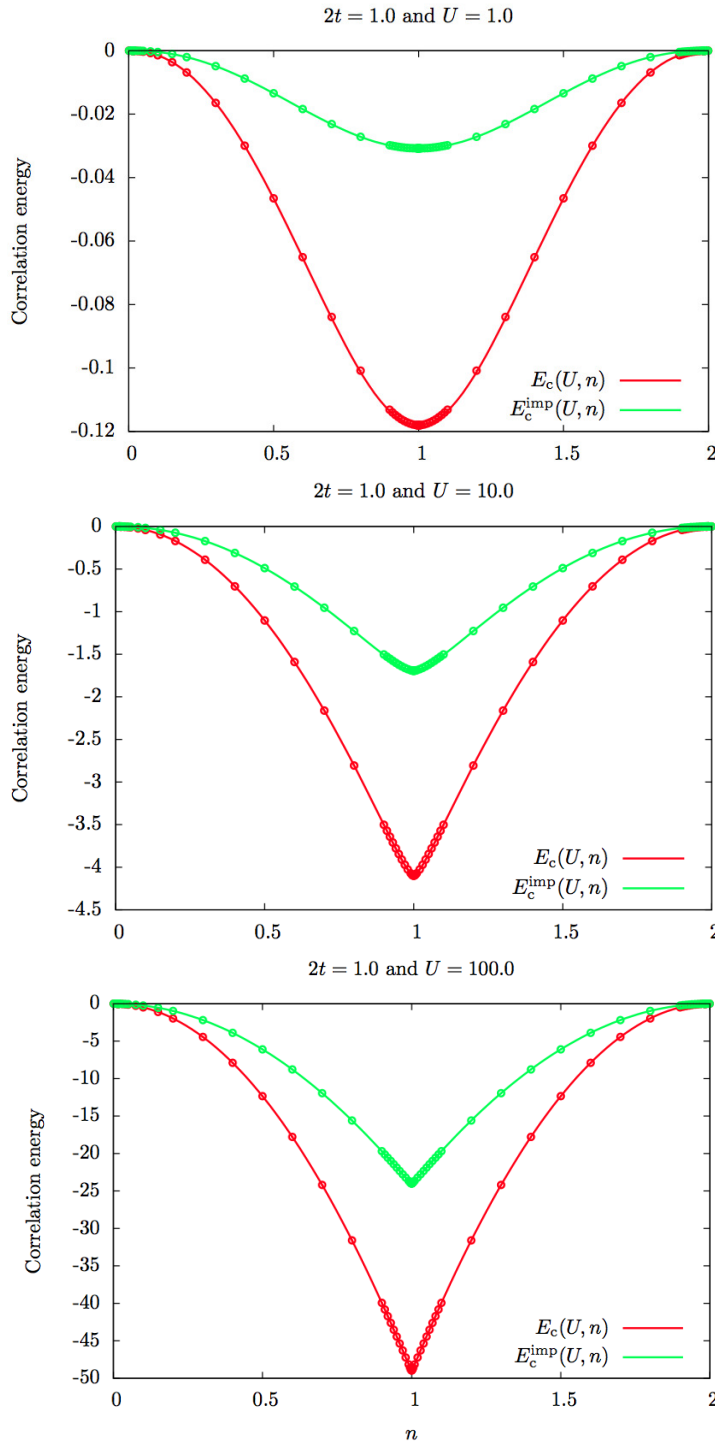


Figure 1. Exact site-occupation functional correlation energies obtained for the embedded impurity and physical (fully-interacting) Hubbard dimer with $U = 1$ (top), $U = 10$ (middle) and $U = 100$ (bottom). Results obtained with the parametrisation of Carrascal *et al.* [46] are shown with open circles. See text for further details.

panel of Figure 2.

The Hubbard dimer is a two-level (2L) system. Therefore, in the following, the superscript "2L" will be used for referring to the impurity correlation functional in Equation (63). In practice, the parametrisation of Ref. [46] can be used with the substitution $U \rightarrow U/2$.

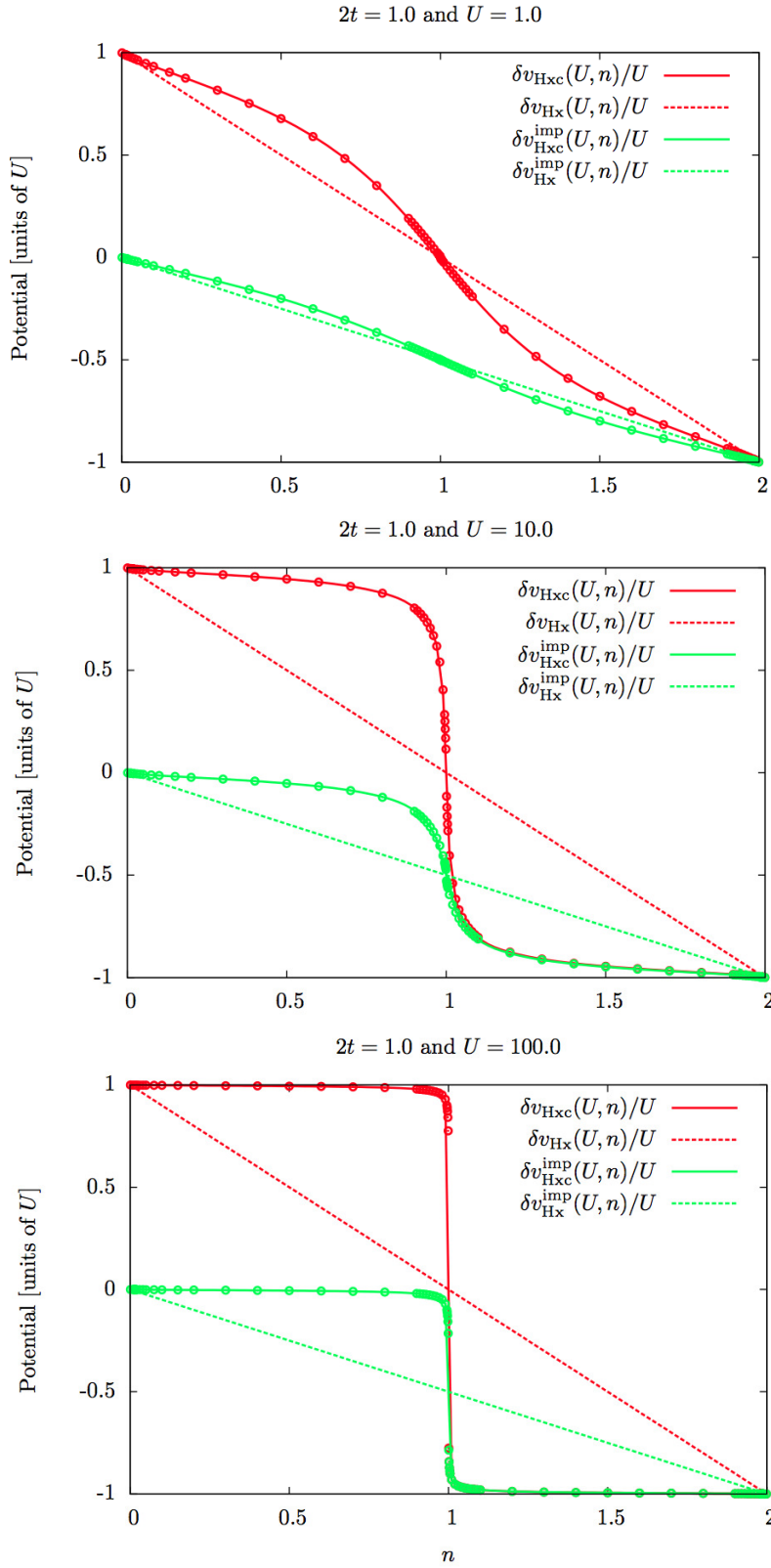


Figure 2. Mean-field (Hx) and exact site-occupation-functional Hxc potentials obtained for the embedded impurity system and the physical (fully-interacting) Hubbard dimer with $U = 1$ (top), $U = 10$ (middle) and $U = 100$ (bottom). Results obtained with the parametrisation of Carrascal *et al.* [46] are shown with open circles. See text for further details.

2.4. Impurity-occupation functional approximation

In order to apply SOET to larger rings or infinite Hubbard systems, approximations to the site-occupation-functional correlation energy of the embedded impurity system must be developed. Their combination with conventional fully-interacting correlation functionals (like the BALDA of Capelle and coworkers [45]) would give approximate site-occupation functionals for the bath (see Equation (19)).

A natural starting point is the LDA which consists in applying SOET to the uniform Hubbard Hamiltonian. In this case, like in the non-uniform case, the impurity correlation energy is in principle a functional of all site occupations (not only the impurity site occupation n_{j_0}). For simplicity, we will assume that it does not vary with the bath site occupations:

$$E_c^{\text{imp}}(\mathbf{n}) \rightarrow E_c^{\text{imp}}(n_{j_0}), \quad (67)$$

and shall refer to this approximation as impurity LDA (ILDA). Let us stress that, for uniform systems, ILDA is an approximation whereas LDA (see Equation (9)) is exact. Indeed, in the uniform case ($v_i = 0$), the exact embedding potential equals, according to Equations (14), (19) and (23),

$$v_i^{\text{emb}} = \frac{U}{2}n_i(1 - \delta_{ij_0}) + \frac{\partial E_c(\mathbf{n})}{\partial n_i} - \frac{\partial E_c^{\text{imp}}(\mathbf{n})}{\partial n_i}, \quad (68)$$

which becomes within ILDA:

$$v_i^{\text{emb}} \rightarrow \frac{U}{2}n_i(1 - \delta_{ij_0}) + \frac{\partial e_c(n_i)}{\partial n_i} - \frac{\partial E_c^{\text{imp}}(n_{j_0})}{\partial n_{j_0}}\delta_{ij_0}. \quad (69)$$

Since, in the exact theory, the occupations are equal ($n_i = n$), we finally obtain the (approximate) ILDA potential expression by shifting the potential in Equation (69) by $-Un/2 - \partial e_c(n)/\partial n$:

$$v_i^{\text{ILDA}} = -\delta_{ij_0} \left(\frac{U}{2}n_{j_0} + \frac{\partial E_c^{\text{imp}}(n_{j_0})}{\partial n_{j_0}} \right). \quad (70)$$

Note that, by definition, the ILDA embedding potential is zero in the bath. As shown numerically in Sec. 4.1, this cannot, in general, lead to strictly uniform site occupations.

Practical ILDA calculations can be performed on a uniform Hubbard system by inserting the above expression into the self-consistent Equation (22), thus leading to

$$\left(\hat{\mathcal{T}} + U\hat{n}_{j_0\uparrow}\hat{n}_{j_0\downarrow} - \left[\frac{U}{2}n_{j_0}^{\Psi^{\text{ILDA}}} + \frac{\partial E_c^{\text{imp}}(n_{j_0}^{\Psi^{\text{ILDA}}})}{\partial n_{j_0}} \right] \hat{n}_{j_0} \right) |\Psi^{\text{ILDA}}\rangle = \mathcal{E}^{\text{ILDA}} |\Psi^{\text{ILDA}}\rangle. \quad (71)$$

In order to turn Equation (71) into a computational method, we need an impurity-occupation correlation functional $E_c^{\text{imp}}(n_{j_0})$. We simply propose to use the functional obtained for the (two-level) Hubbard dimer, which gives, according to Equations

tion (63),

$$E_c^{\text{imp}}(n_{j_0}) \rightarrow E_c^{2\text{L}}(U/2, n_{j_0}). \quad (72)$$

This approximation will be referred to as 2L-ILDA. For comparison, we discuss in the following the computation of an approximate Legendre–Fenchel transform (see Equation (12)) where the potential is set to zero in the bath, in analogy with ILDA:

$$F^{\text{imp}}(\mathbf{n}) \rightarrow \sup_{v_{j_0}} \{ \mathcal{E}^{\text{imp}}(v_{j_0}) - v_{j_0} n_{j_0} \}. \quad (73)$$

The maximising potential in Equation (73) will be referred to as impurity-optimised potential in the following.

3. Computational details

As a proof of concept, SOET has been applied to the uniform 8-site Hubbard ring ($L = 8$) with periodic or antiperiodic boundary conditions. The number of electrons N will always be even and will vary from 2 to 14. In order to remove the pathological degeneracy, we follow the standard treatment of the boundary conditions: In the case of $N = 2, 6, 10, 14$, we adopt the periodic boundary condition ($\hat{a}_{L+1,\sigma} = \hat{a}_{1,\sigma}$), and in the case of $N = 4, 8, 12$, we adopt the antiperiodic boundary condition ($\hat{a}_{L+1,\sigma} = -\hat{a}_{1,\sigma}$). Legendre–Fenchel transforms in Equations (12) and (73) have been implemented as well as the 2L-ILDA (see Equations (71) and (72)). In the latter case, the parametrisation of Carrascal *et al.* [46] (see Equations (102)–(107) in their paper) has been used for the correlation functional of the dimer. Exact diagonalisations (FCI) based on the Lanczos algorithm [51] have been used in all models. The convergence threshold was set to 10^{-6} for the site occupations. Exact impurity correlation energies were computed as follows,

$$E_c^{\text{imp}}(\mathbf{n}) = F^{\text{imp}}(\mathbf{n}) - \mathcal{T}_s(\mathbf{n}) - \frac{U}{4} n_{j_0}^2. \quad (74)$$

Note that the embedded impurity Legendre–Fenchel transform in Equation (12) reduces to the non-interacting kinetic energy when $U = 0$. The hopping parameter was set to $t = 1/2$. Various correlation regimes have been investigated ($U = 1, 10$, and 100).

4. Results and discussion

4.1. Exact embedding potentials

The so-called v -representability of given site occupations [44, 52] is usually considered for fully-interacting or non-interacting systems. Since SOET relies on a fictitious embedded impurity system, the problem of what could be referred to as impurity-interacting v -representability arises. In other words, is it always possible to find a potential such that the embedded impurity system has the desired site occupations? This question is relevant even for uniform site occupations. In the latter case, the answer is trivial for both non-interacting and fully-interacting systems: the potential is a constant. This cannot be true anymore if an impurity is introduced into the system. As shown in Figure 3, embedding potentials can be

computed very accurately by means of Legendre–Fenchel transforms for various uniform site occupations in the 8-site Hubbard ring. These potentials will be referred to as exact embedding potentials in the following. As expected, the difference in potential between the impurity site and the bath is substantial. Moreover, the potential is not strictly uniform in the bath, even though the difference in potential between two bath sites seems to be relatively small. From this observation we conclude that ILDA is a sound approximation. Interestingly, at half-filling ($N = 8$), ILDA becomes exact and the potential in the bath reduces to its mean-field approximation. Note that this feature has already been observed in the Hubbard dimer (see Figure 2).

Another important feature of the exact embedding potential is the discontinuity at half-filling in the strongly correlated limit ($U \rightarrow +\infty$), as highlighted in Figure 4. Let us stress that a similar pattern is obtained in the Hubbard dimer (see Figure 2). In this respect, 2L-ILDA, which relies on ILDA and the two-level Hubbard model, is also a sound approximation.

For analysis purposes, approximate Legendre–Fenchel transforms have been computed with the potential set to zero in the bath (see Equation (73)), thus leading to impurity-optimised embedding potentials. The corresponding site occupations are shown in Figure 5. In the weakly correlated regime ($U = 1$), they are almost uniform. Fluctuations around the exact uniform occupations are shown in Figure 7. When U increases, the deviation from uniformity is more visible, simply because the bath does not contribute to the impurity-optimised potential. Nevertheless, even for the large $U = 100$ value, such a potential provides a good starting point for better approximations. In this respect, ILDA is also relevant in the strongly correlated regime. Note that the impurity-optimised potential is the best potential one can get within ILDA since it reproduces the impurity occupation exactly.

4.2. Two-level ILDA results

This section deals with the performance of the 2L-ILDA. Converged site occupations are shown in Figure 6. 2L-ILDA is exact at half-filling ($N = 8$), as expected. Indeed, in this case, the potential is uniform in the bath and equal to its mean-field approximation. Away from half-filling, site occupations deviate from uniformity. Comparison is made with the impurity-optimised potential results in Figure 7 for $N = 6$ electrons. 2L-ILDA does not reproduce the correct impurity occupation whereas, by construction, the impurity-optimised potential scheme does. This was somehow expected since the site-occupation-functional embedding potential used in the 2L-ILDA is parametrised for the Hubbard dimer. In the latter case, if the impurity occupation is n , the potential will impose the occupation $2 - n$ on the other site. In other words, we cannot expect 2L-ILDA to provide strict uniformity. For analysis purposes, the convergence of the site occupations is shown in Figure 8. Note that it is smooth. At iteration 0, the impurity occupation is set to the expected uniform value $N/8$. The site occupations become non-uniform already at the first iteration in the self-consistent calculation of the 2L-ILDA potential. The standard deviation from uniformity,

$$\sigma = \sqrt{\sum_{i=1}^L \frac{(n_i - N/L)^2}{L}}, \quad (75)$$

is plotted in Figure 9 with respect to U . It increases monotonically with U . The largest slope is obtained in the range $0 < U < 10$. Then the slope decreases

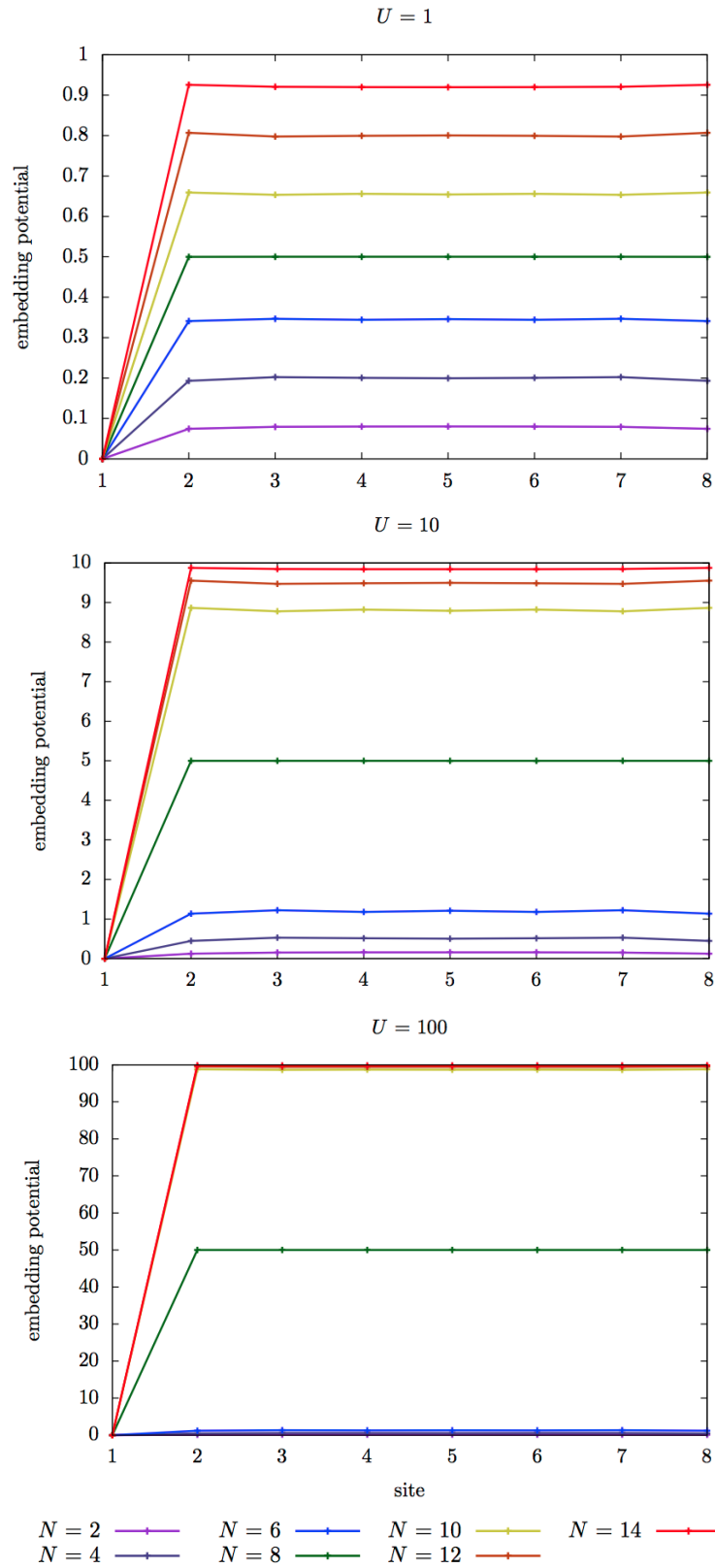


Figure 3. Exact embedding potentials obtained for uniform 8-site Hubbard rings with $U = 1$ (top), $U = 10$ (middle) and $U = 100$ (bottom). The site occupations are $N/8$ where N is the number of electrons. The impurity site is labelled as 1. Potentials are set to zero on the impurity site.

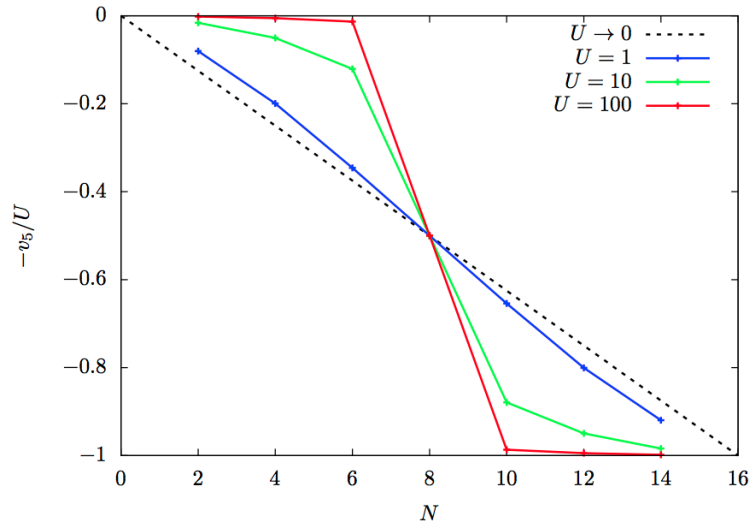


Figure 4. Exact embedding potentials in the bath (site 5) obtained for uniform 8-site Hubbard rings with $U = 1$, $U = 10$ and $U = 100$. The site occupations are $N/8$ where N is the number of electrons. Potentials are set to zero on the impurity site. Comparison is made with the mean-field approximation ($U \rightarrow 0$).

significantly for $10 < U < 30$. In the strongly correlated regime ($U > 30$), the standard deviation becomes less sensitive to the repulsion strength.

Let us now focus on the 2L-ILDA embedding potential. Comparison is made with the exact and impurity-optimised potentials in Figure 10. A nice feature of 2L-ILDA is that the step that leads to a discontinuity at half-filling in the $U/t \rightarrow +\infty$ limit is relatively well reproduced. In the weakly correlated regime ($U = 1$), self-consistency does not affect the potential significantly which is relatively close to the exact one. This statement does not hold for $U = 10$. This can be related to the deviation from uniformity discussed previously.

Turning to the impurity correlation energy (see Figure 11), comparison with the exact and 2L-ILDA (iteration 0) results shows that the error is, like in many conventional DFT calculations [53], essentially driven by the approximate functional when U is small. This was expected since the impurity correlation functional used in 2L-ILDA is parametrised for the Hubbard dimer where the bath reduces to a single site with occupation $2 - n$ rather than a collection of sites which all have the same occupation n . On the other hand, when the correlation is strong ($U = 10$ and $U = 100$), the error is site-occupation-driven. Indeed, at iteration 0, the impurity occupation is exact and the 2L-ILDA impurity correlation energy is close to the exact one. This is probably due to the fact that, in the strongly correlated limit, interactions become essentially local. As mentioned previously, self-consistency deteriorates the impurity occupation, thus leading to a substantial error in the correlation energy.

5. Conclusion

The extension of DFT to model Hamiltonians such as the Hubbard Hamiltonian, as well as the formulation of an exact site-occupation embedding theory (SOET), which was recently proposed by one of the authors [41], have been briefly reviewed. A simple local site-occupation approximation, referred to as 2L-ILDA, has then been proposed in order to perform practical SOET calculations. It relies on two approximations: (i) the correlation energy of the embedded impurity system is

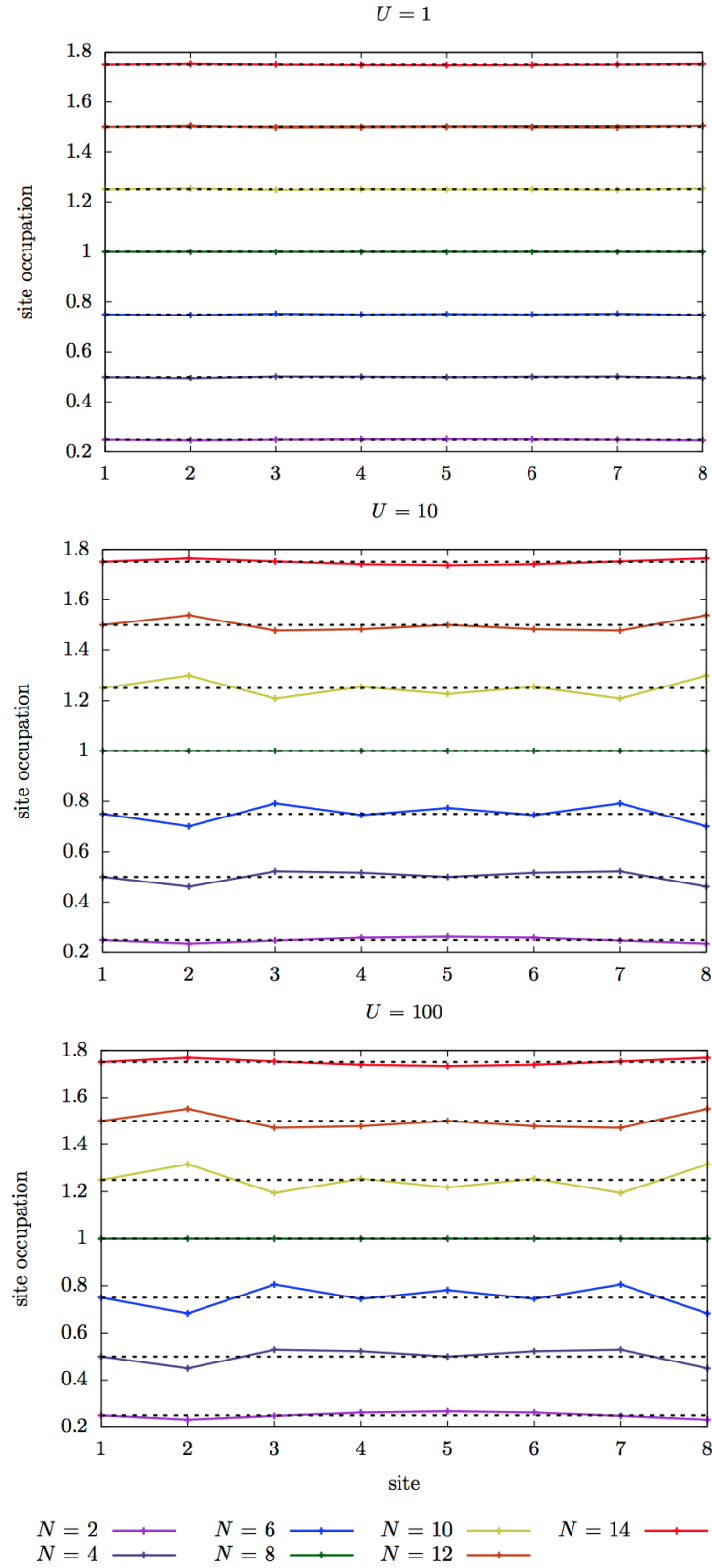


Figure 5. site occupations obtained with the impurity-optimised potential for uniform 8-site Hubbard rings with $U = 1$ (top), $U = 10$ (middle) and $U = 100$ (bottom). N is the number of electrons. The impurity site is labelled as 1. Dashed lines show uniform site occupations. See text for further details.

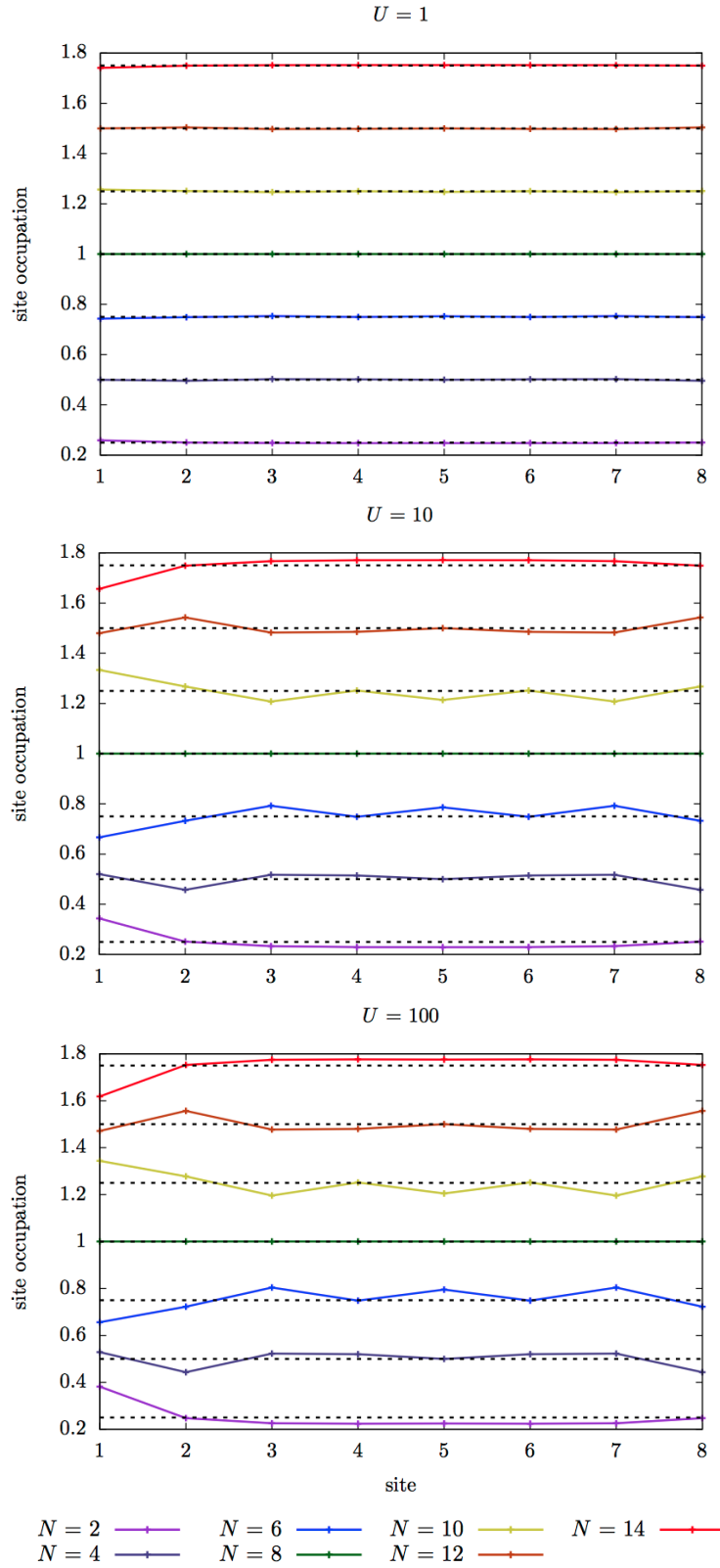


Figure 6. site occupations obtained self-consistently with the 2L-ILDA potential for uniform 8-site Hubbard rings with $U = 1$ (top), $U = 10$ (middle) and $U = 100$ (bottom). N is the number of electrons. The impurity site is labelled as 1. Dashed lines show uniform site occupations. See text for further details.

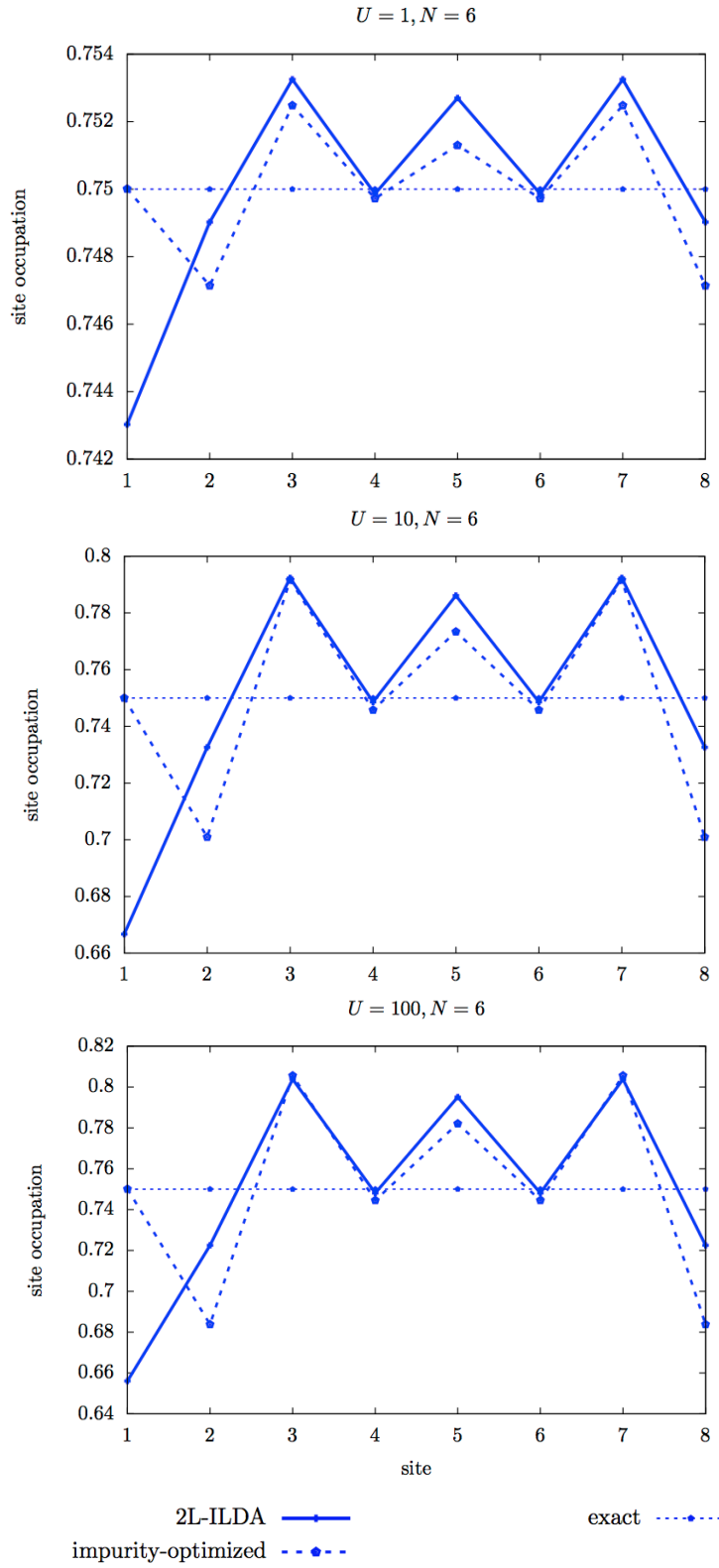


Figure 7. site occupations obtained with the exact, impurity-optimised and self-consistent 2L-ILDA embedding potentials for the uniform 8-site Hubbard ring with 6 electrons and $U = 1$ (top), $U = 10$ (middle) and $U = 100$ (bottom). The impurity site is labelled as 1.

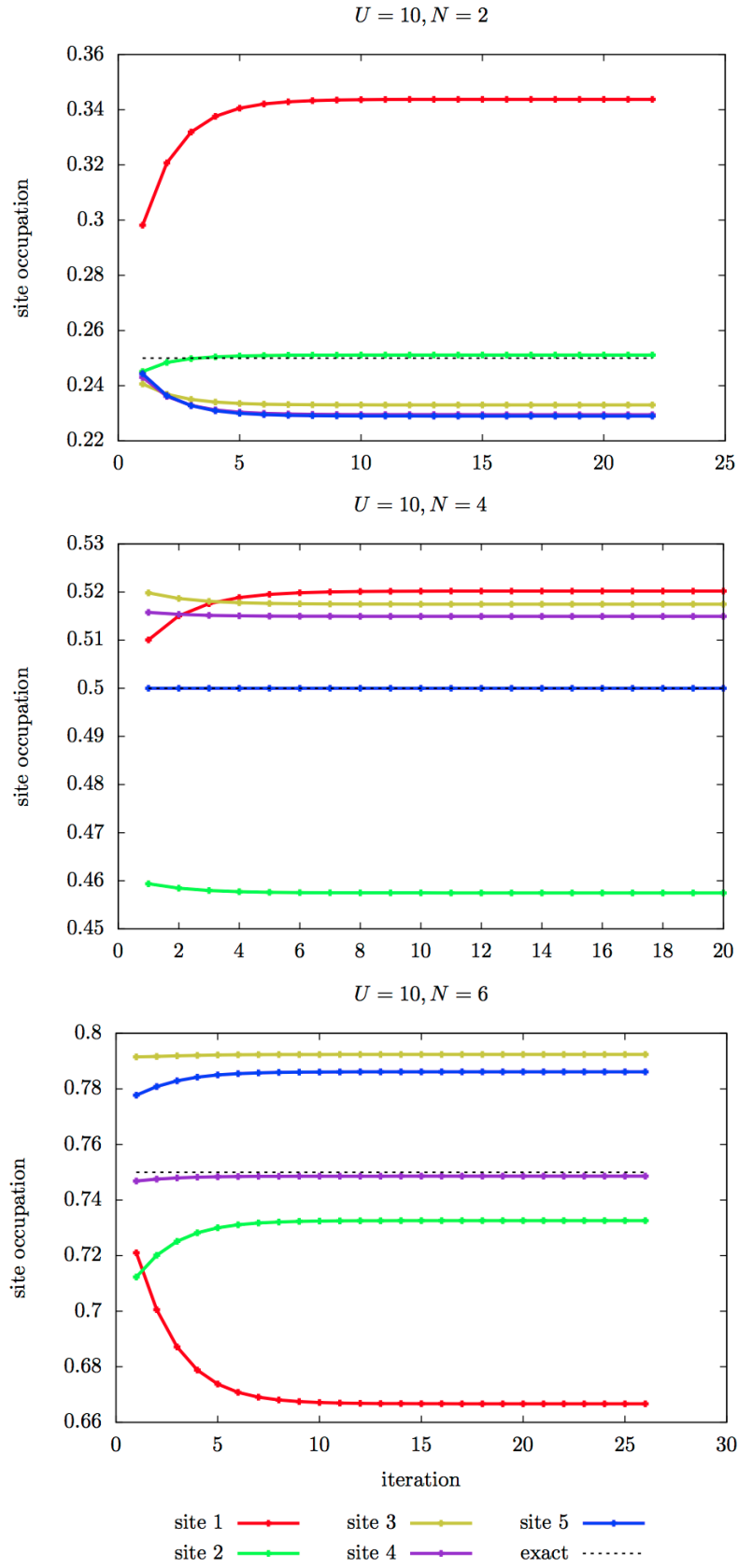


Figure 8. Convergence of the site occupations in self-consistent 2L-ILDA calculations for uniform 8-site Hubbard rings with $N = 2$ (top), $N = 4$ (middle) and $N = 6$ (bottom) electrons. The U parameter is set to 10. The impurity site is labelled as 1.

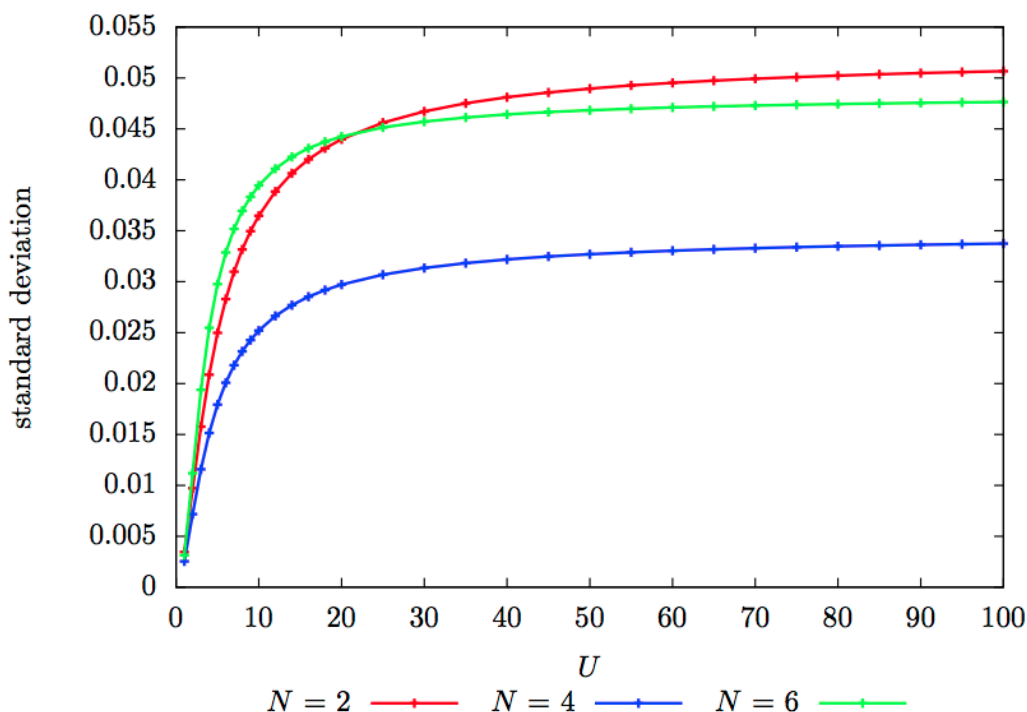


Figure 9. Standard deviation of converged 2L-ILDA site occupations obtained when varying U in uniform 8-site Hubbard rings with $N = 2$, $N = 4$ and $N = 6$ electrons. See text for further details.

assumed to depend on the occupation of the impurity site only and, within such an approximation, (ii) the embedded impurity correlation functional of the (two-level) Hubbard dimer is employed. As a proof of concept, the theory has been tested on a uniform 8-site Hubbard ring. Exact and 2L-ILDA calculations have been performed. In the latter case, the parametrisation of Carrascal *et al.* [46] has been used. Promising results were obtained at the 2L-ILDA level, even though the approximation is quite simple. In the weakly correlated regime, the error on the impurity correlation energy is functional-driven while, in the strongly correlated regime, it is site-occupation-driven. Results might be improved by developing a functional that depends explicitly on the impurity nearest neighbours occupations, in the spirit of the generalised gradient approximation in DFT. The Anderson model [54] might be used for developing more accurate ILDA schemes. In order to turn SOET into a useful computational method, one should obviously compute double occupancies, through the evaluation of energy derivatives with respect to the on-site repulsion parameter U , and perform calculations on larger rings, for example, by combining DMRG [12] with SOET. Note finally that SOET can in principle be applied to quantum chemical Hamiltonians. As a first step, it might be interesting to consider the Richardson Hamiltonian [55]. Work is currently in progress in all these directions.

Acknowledgements

The authors are pleased to dedicate this work to Hans Jørgen Aagaard Jensen on the occasion of his 60th birthday (congratulations Hans Jørgen and thanks for everything !). They would like to thank Andreas Savin, Antonin Hommes, Killian Deur and Laurent Mazouin for fruitful discussions. E. Fromager acknowledges financial support from the LABEX 'Chemistry of complex systems' [grant

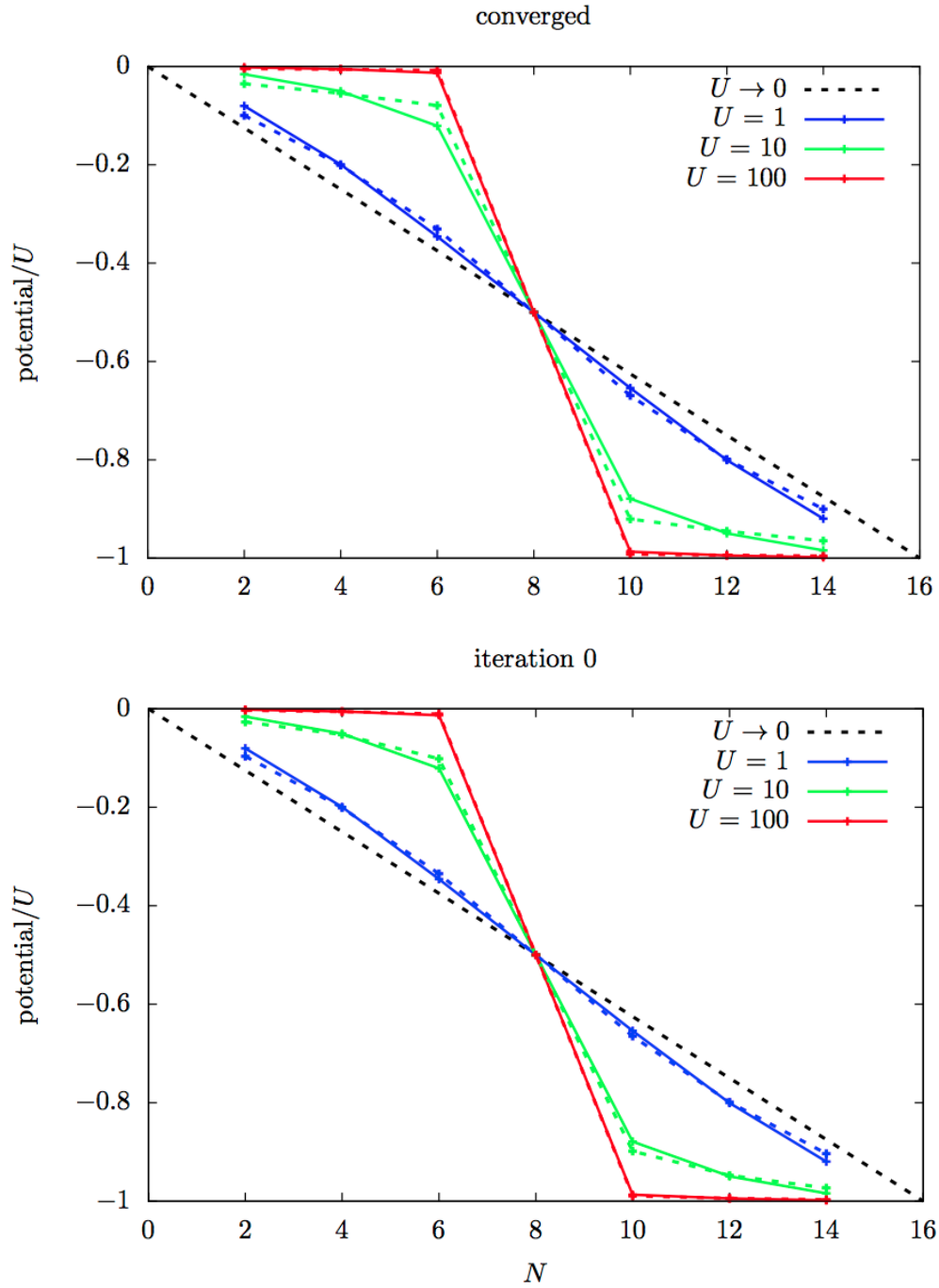


Figure 10. Impurity-optimised (solid lines) and 2L-ILDA (dashed lines) embedding potentials obtained for $U = 1$, $U = 10$ and $U = 100$ when varying the number N of electrons in a uniform 8-site Hubbard ring. Converged (top) and non-converged (bottom) 2L-ILDA potentials are shown. The exact (see Figure 4) and impurity-optimised potentials were found to be on top of each other. The mean-field approximation ($U \rightarrow 0$) is also shown for comparison.

number CSC-VRO-13] and the ANR (MCFUNEX project [grant number ANR-14-CE06-0014-01]). B. Senjean thanks the Ecole Doctorale des Sciences Chimiques in Strasbourg for his PhD grant.

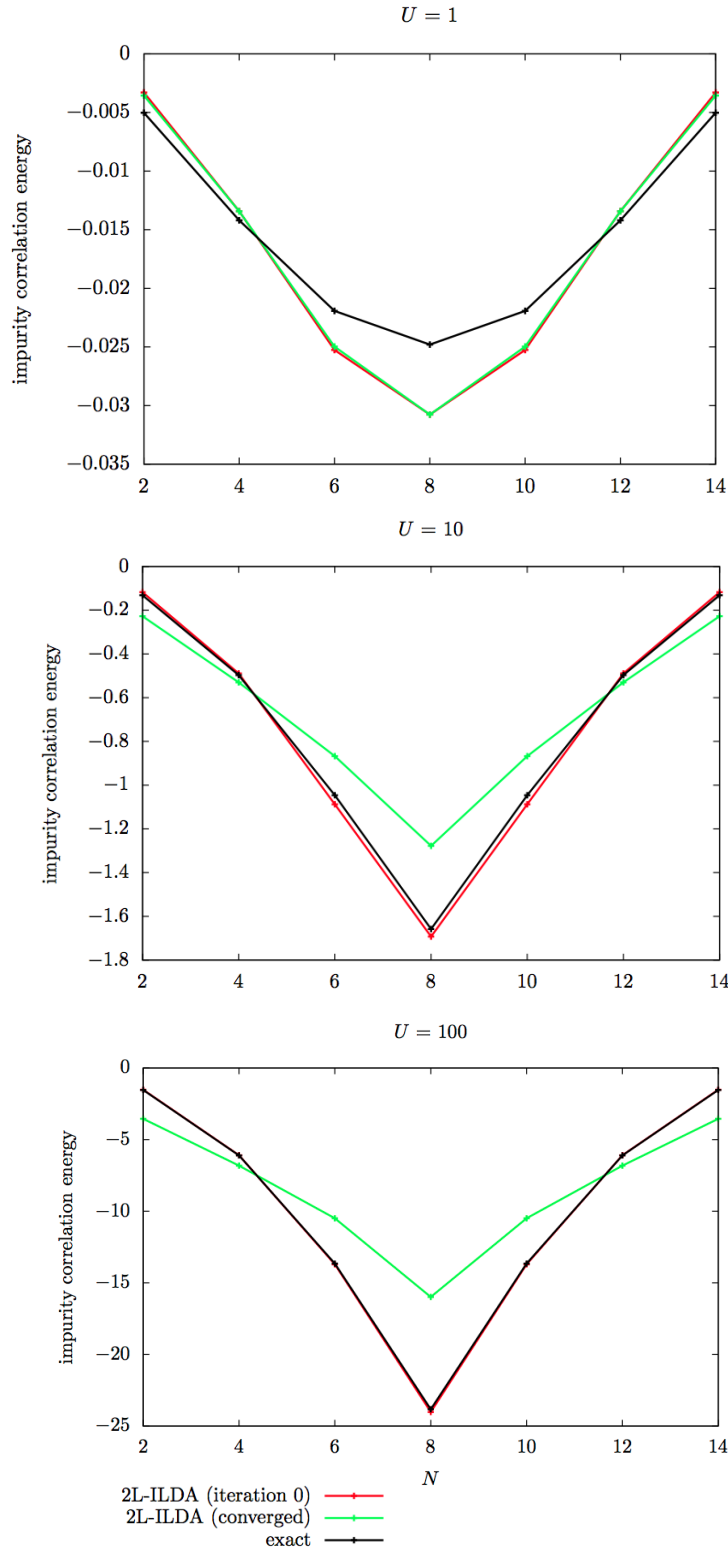


Figure 11. Exact and 2L-ILDA impurity correlation energies obtained for $U = 1$ (top), $U = 10$ (middle) and $U = 100$ (bottom) when varying the number N of electrons in a uniform 8-site Hubbard ring. Converged and non-converged 2L-ILDA results are shown. In the latter case, the impurity site occupation is set to the expected exact value $N/8$.

References

- [1] K. Andersson, P.Å. Malmqvist and B.O. Roos, *J. Chem. Phys.* **96** (2), 1218 (1992).
- [2] D. Roca-Sanjuán, F. Aquilante and R. Lindh, *WIREs Comput Mol Sci* **2** (4), 585 (2012).
- [3] C. Angeli, R. Cimiraglia, S. Evangelisti, T. Leininger and J.P. Malrieu, *J. Chem. Phys.* **114** (23), 10252 (2001).
- [4] C. Angeli, R. Cimiraglia and J.P. Malrieu, *J. Chem. Phys.* **117** (20), 9138 (2002).
- [5] D.I. Lyakh, M. Musiał, V.F. Lotrich and R.J. Bartlett, *Chem. Rev.* **112** (1), 182 (2011).
- [6] C. Gros, R. Joynt and T. Rice, *Phys. Rev. B* **36** (1), 381 (1987).
- [7] S. Sorella, *Phys. Rev. B* **71** (24), 241103 (2005).
- [8] E. Neuscamman, C. Umrigar and G.K.L. Chan, *Phys. Rev. B* **85** (4), 045103 (2012).
- [9] S. Zhang, J. Carlson and J. Gubernatis, *Phys. Rev. Lett.* **78** (23), 4486 (1997).
- [10] C.C. Chang and S. Zhang, *Phys. Rev. Lett.* **104** (11), 116402 (2010).
- [11] T. Yanagisawa, S. Koike and K. Yamaji, *Phys. Rev. B* **64** (18), 184509 (2001).
- [12] S.R. White, *Phys. Rev. Lett.* **69**, 2863 (1992).
- [13] S.R. White, *Phys. Rev. B* **48** (14), 10345 (1993).
- [14] R. Rodríguez-Guzmán, C.A. Jiménez-Hoyos, R. Schutski and G.E. Scuseria, *Phys. Rev. B* **87** (23), 235129 (2013).
- [15] G.E. Scuseria, C.A. Jiménez-Hoyos, T.M. Henderson, K. Samanta and J.K. Ellis, *J. Chem. Phys.* **135** (12), 124108 (2011).
- [16] C.A. Jiménez-Hoyos, T.M. Henderson, T. Tsuchimochi and G.E. Scuseria, *J. Chem. Phys.* **136** (16), 164109 (2012).
- [17] R. Rodríguez-Guzmán, K. Schmid, C.A. Jiménez-Hoyos and G.E. Scuseria, *Phys. Rev. B* **85** (24), 245130 (2012).
- [18] O. Juillet and R. Frésard, *Phys. Rev. B* **87** (11), 115136 (2013).
- [19] N. Tomita, *Phys. Rev. B* **69** (4), 045110 (2004).
- [20] D. Baeriswyl, D. Eichenberger and M. Menteshashvili, *New. J. Phys.* **11** (7), 075010 (2009).
- [21] N. Lanata, H.U. Strand, X. Dai and B. Hellsing, *Phys. Rev. B* **85** (3), 035133 (2012).
- [22] P. Pulay, *Chem. Phys. Lett.* **100** (2), 151 (1983).
- [23] S. Saebo and P. Pulay, *Annu. Rev. Phys. Chem.* **44** (1), 213 (1993).
- [24] C. Hampel and H.J. Werner, *J. Chem. Phys.* **104** (16), 6286 (1996).
- [25] T. Tsuchimochi, M. Welborn and T. Van Voorhis, *J. Chem. Phys.* **143** (2), 024107 (2015).
- [26] A. Georges, G. Kotliar, W. Krauth and M.J. Rozenberg, *Rev. Mod. Phys.* **68** (1996).
- [27] G. Kotliar and D. Vollhardt, *Phys. Today* **57** (3), 53 (2004).
- [28] G. Kotliar, S.Y. Savrasov, K. Haule, V.S. Oudovenko, O. Parcollet and C.A. Marianetti, *Rev. Mod. Phys.* **78**, 865 (2006).
- [29] K. Held, *Adv. Phys.* **56** (6), 829 (2007).
- [30] D. Zgid and G.K.L. Chan, *J. Chem. Phys.* **134** (2011).
- [31] A.A. Kananenka, E. Gull and D. Zgid, *Phys. Rev. B* **91** (12), 121111 (2015).
- [32] T.N. Lan, A.A. Kananenka and D. Zgid, *J. Chem. Phys.* **143** (24), 241102 (2015).
- [33] N.E. Dahlen and R. van Leeuwen, *J. Chem. Phys.* **122** (16), 164102 (2005).
- [34] J.J. Phillips and D. Zgid, *J. Chem. Phys.* **140** (24), 241101 (2014).
- [35] G. Knizia and G.K.L. Chan, *Phys. Rev. Lett.* **109**, 186404 (2012).
- [36] B.X. Zheng and G.K.L. Chan, *Phys. Rev. B* **93** (3), 035126 (2016).
- [37] I.W. Bulik, G.E. Scuseria and J. Dukelsky, *Phys. Rev. B* **89**, 035140 (2014).
- [38] K.i. Nakamura, *Prog. Theor. Phys.* **21** (5), 713 (1959).
- [39] W. Kutzelnigg, *J. Chem. Phys.* **40** (12), 3640 (1964).
- [40] A. Coleman, *J. Math. Phys.* **6** (9), 1425 (1965).
- [41] E. Fromager, *Mol. Phys.* **113** (5), 419 (2015).
- [42] O. Gunnarsson and K. Schönhammer, *Phys. Rev. Lett.* **56** (18), 1968 (1986).
- [43] K. Capelle and V.L. Campo Jr., *Phys. Rep.* **528**, 91 (2013).
- [44] K. Schonhammer, O. Gunnarsson and R. Noack, *Phys. Rev. B* **52**, 2054 (1995).
- [45] K. Capelle, N.A. Lima, M.F. Silva and L.N. Oliveira, *Phys. Rev. Lett.* **90**, 146402 (2003).
- [46] D.J. Carrascal, J. Ferrer, J.C. Smith and K. Burke, *J. Phys. Condens. Matter* **27** (39), 393001 (2015).
- [47] E.H. Lieb, *Int. J. Quantum Chem.* **24** (3), 243 (1983).
- [48] J.P. Bergfield, Z.F. Liu, K. Burke and C.A. Stafford, *Phys. Rev. Lett.* **108** (6), 066801 (2012).
- [49] Z.F. Liu, J.P. Bergfield, K. Burke and C.A. Stafford, *Phys. Rev. B* **85** (15), 155117 (2012).
- [50] Z.F. Liu and K. Burke, *Phys. Rev. B* **91** (24), 245158 (2015).
- [51] E. Dagotto, *Rev. Mod. Phys.* **66**, 763 (1994).
- [52] A. Schindlmayr and R. Godby, *Phys. Rev. B* **51** (16), 10427 (1995).
- [53] M.C. Kim, E. Sim and K. Burke, *Phys. Rev. Lett.* **111** (7), 073003 (2013).
- [54] P.W. Anderson, *Phys. Rev.* **124**, 1 (1961).
- [55] P.A. Johnson, P.W. Ayers, P.A. Limacher, S. De Baerdemacker, D. Van Neck and P. Bultinck, *Comp. Theor. Chem.* **1003**, 101 (2013).